Determination of the Phase Equilibria in the Mn-Sn-Zn System at 500 °C

J.L. LIANG, Y. DU, Q.Z. ZHAO, C.Z. LIAO, Y.Y. TANG, L.M. ZENG, W.W. ZHANG, and H.H. XU

The isothermal section of the Mn-Sn-Zn system at 500 °C was determined with 20 alloys. The alloys were prepared by melting the pure elements in evacuated quartz capsules. The alloy samples were examined by means of X-ray diffraction (XRD) and scanning electron microscopy coupled with energy-dispersive X-ray spectroscopy. A new ternary phase Mn_4Zn_8Sn (λ) was found to have a bcc structure with a lattice parameter $a = 0.92508$ (5) nm. Its composition range spans 25 to 35 at. pct Mn, 4 to 8 at. pct Sn, and 55 to 70 at. pct Zn. The Zn is substituted for Mn in Mn_3Sn, Mn_2Sn, and Mn_3Sn_2. The solubility of Zn in Mn_3Sn, Mn_2Sn, and Mn_3Sn_2 was measured to be about 17, 12, and 4 at. pct, respectively. The phase boundaries of the liquid and β-Mn phases were well established. The following 3 three-phase equilibria were well determined: (1) β-Mn + ε-$MnZn_3$ + Mn_3Sn, (2) λ + Mn_3Sn + Mn_2Sn, and (3) L + λ + Mn_2Sn. The additional 5 three-phase equilibria, which are ε-$MnZn_3$ + λ + Mn_3Sn, ε_1-$MnZn_3$ + ε-$MnZn_3$ + λ, ε_1-$MnZn_3$ + λ + L, Mn_2Sn + L + $MnSn_2$, and Mn_3Sn_2 + $MnSn_2$ + Mn_2Sn, were deduced and shown with dashed lines in the present isothermal section.

DOI: 10.1007/s11661-009-0026-8

I. INTRODUCTION

THE hot-dip zinc coatings are widely used to protect steel components exposed to corrosive environments. To improve the coating properties, alloying elements, such as Al,[1] Ni,[2] Mn,[3] Sn,[4] and Ti,[5] are added to the molten Zn bath. It was reported that the addition of Ni and Al in the molten bath suppresses the Sandelin effect[6] that is referred as the coatings grow over thickness during the galvanizing of the Si-bearing steel. Knowledge of the interactions among alloying elements, Zn liquid, and Fe is desirable for the advanced development of the hot-dip galvanizing process. For example, the Fe-Al-Zn phase diagram has been applied effectively in the galvanizing industry to the determination of effective Al content in the molten bath, the control of dross generation, and the prediction of the Al consumption.[7]

Several galvanizing related ternary systems such as Fe-Ni-Zn,[8] Fe-Sn-Zn,[9] Fe-Ti-Zn,[10] Fe-Al-Zn,[11] Fe-Mn-Zn,[12] Fe-Cr-Zn,[13] Zn-Bi-Ni,[14] and Zn-Al-Mo[15] were experimentally investigated. In addition, the phase equilibria in some quaternary systems such as Zn-Fe-Ni-Ti[16] and Zn-Fe-Ni-Si[17] were also experimentally studied. So far, however, no information on the phase relationship in the Mn-Sn-Zn system is available in the literature. The purpose of the present work is to determine the isothermal section at 500 °C of the Mn-Sn-Zn system.

The three binary phase diagrams in the Mn-Sn-Zn system have been reasonably established. Okamoto and Tanner[18] reported an assessed Mn-Zn phase diagram based on the previously published literature, as shown in Figure 1(a). They proposed the existence of three phase subdivisions (ε, ε_1, and ε_2) of the ε phase ($MnZn_3$) mainly based on the work of Wachtel and Tsiuplakis.[19] However, the experimental investigations[20–24] published former and later on this system showed no indication of phase separation. In a recent experimental investigation of the Mn-Si-Zn system using diffusion couple techniques, one of the authors confirmed that the $MnZn_3$ region consisted of two subdivisions (ε and ε_1).[25] In the present work, this conclusion is accepted.

The Mn-Sn system[26] has four intermediate phases, *viz*. $MnSn_2$, Mn_2Sn, Mn_3Sn, and Mn_3Sn_2. It was revealed that the low-temperature phase Mn_3Sn_2 has an orthorhombic structure.[26, 27] The revised Mn-Sn phase diagram from Reference 26 is redrawn in Figure 1(b).

The Sn-Zn phase diagram[28] is of the simple eutectic type, as shown in Figure 1(c). The eutectic reaction, L → Sn + Zn, occurs at 85.6 at. pct Sn and 198.5 °C.

J.L. LIANG, Doctoral Candidate, is with the State Key Laboratory of Powder Metallurgy, Central South University, Changsha, Hunan 410083, People's Republic of China, and now also the Associated Professor of the Institute of Materials Science, College of Physics and Electronic Engineering, Guangxi University for Nationalities, Nanning, Guangxi, 530006, People's Republic of China. Y. DU and H.H. XU, Professors, and W.W. ZHANG, Master Candidate, are with the State Key Laboratory of Powder Metallurgy, Central South University. Contact e-mail: yongduyong@gmail.com Q.Z. ZHAO, Undergraduate Student, and Y.Y. TANG, Lecturer, are with the Institute of Materials Science, College of Physics and Electronic Engineering, Guangxi University for Nationalities. C.Z. LIAO, Master Candidate, and L.M. ZENG, Professor, are with the Key Laboratory of Nonferrous Metals and New Processing Technology of Materials, Ministry of Education (Guangxi University).

Manuscript submitted September 5, 2008.
Article published online October 14, 2009

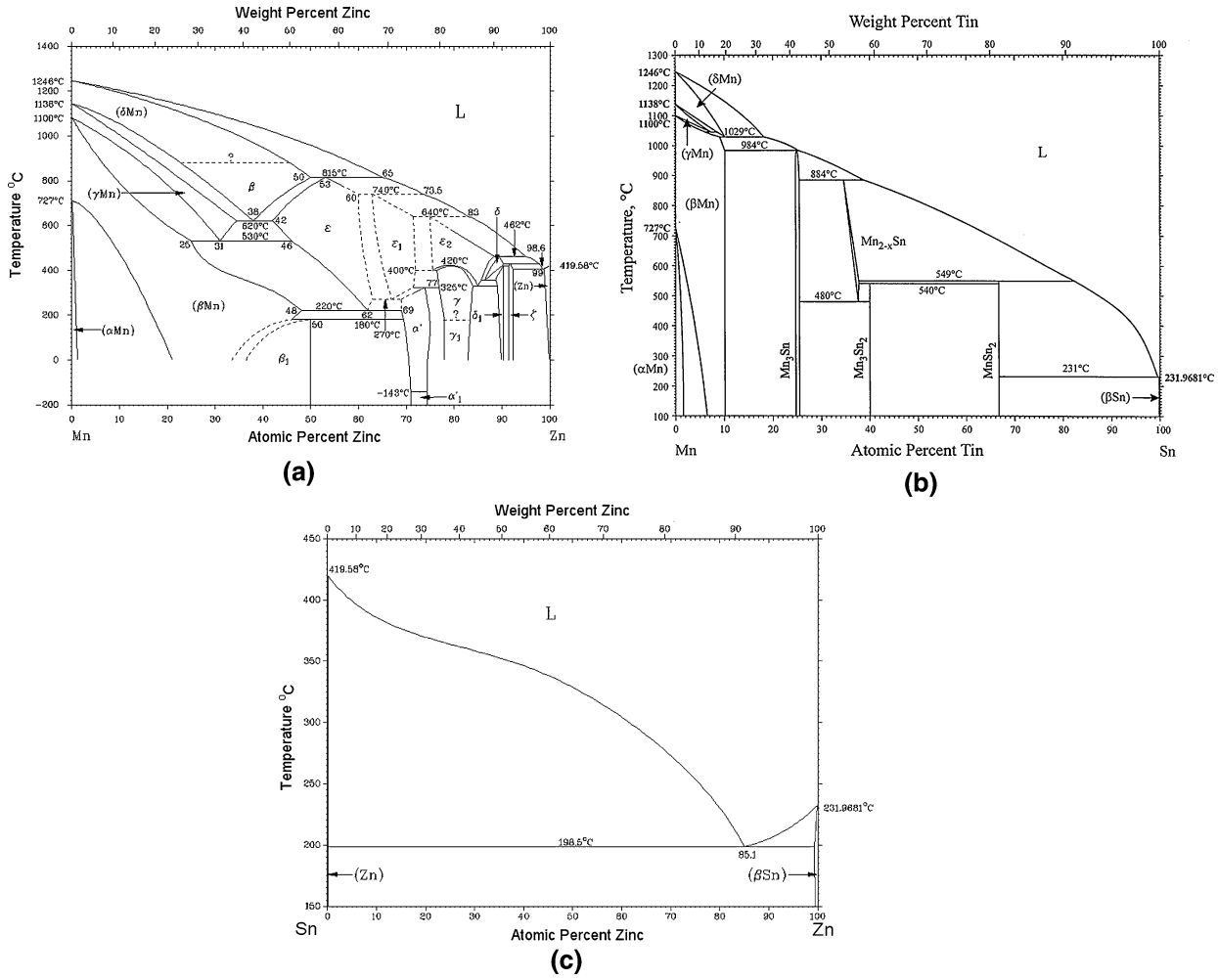

Fig. 1—Phase diagrams of three binary systems: (*a*) Mn-Zn,[18] (*b*) Mn-Sn,[26] and (*c*) Sn-Zn.[28]

II. EXPERIMENTAL PROCEDURES

Pure metals of Mn (99.9 pct), Sn (99.9 pct), and Zn (99.9 pct) were used as starting materials. Twenty alloys were prepared by sealing the accurately weighed ingredients in evacuated quartz tubes and then heating to a temperature sufficiently above the liquidus. To improve the homogeneity of the molten alloys, the quartz tubes were shaken and inversed several times, followed by furnace cooling. The alloy ingots, which were separately wrapped with Ta foils, were encapsulated in quartz tubes and then annealed at 500 °C for 20 days. After completion of annealing, the alloys were quenched in cold water without breaking the quartz tubes.

X-ray diffraction (XRD) analysis was conducted using an XD-3 diffractometer (Beijing Purkinje General Instrument Co., Beijing) with Cu K_α radiation and Ni foil filter, operating at 40 kV and 30 mA.

Several alloys were annealed again at 500 °C for additional 20 days. The XRD results showed that the prolonged heat treatment up to 40 days produced the same phase assemblage as those of 20 days.

During the preparation of this article, the XD-3 diffratometer was newly equipped with a graphite monochrome. Some alloys, which had been kept at room temperature for 9 months, were subjected to XRD again. The decrease of the XRD background with the use of the graphite monochrome makes the phase identification more reliable.

The microstructure observation and composition analysis of the metallographic alloy samples were carried out with the S-3400N scanning electron microscope (SEM, Hitachi Ltd., Tokyo) coupled with energy-dispersive X-ray spectroscopy (EDS) (EDAX Inc., Mahwah, NJ). Conventional matrix correction to the EDS measurements, which treats the deviation from linearity by including the effects of atomic number (Z), absorption (A), and fluorescence (F) (ZAF), was used to calculate the compositions from the measured X-ray intensities for Mn K_α, Sn L_α, and Zn K_α. The error was estimated to be within about 2 at. pct.

III. RESULTS AND DISCUSSION

Table I gives the compositions of the alloys and the phases and phase equilibrium data determined by a

Table I. Summary of the Phase Identification and Its Compositions for the Mn-Sn-Zn Alloys Annealed at 500 °C for 20 Days

	Composition (At. Pct)							Phase Composition (At. Pct)		
	Nominal			Measured by EDS				Measured by EDS		
Number	Mn	Zn	Sn	Mn	Zn	Sn	Phase Identified by XRD	Mn	Zn	Sn
1	50	40	10	49.3	39.9	10.8	Mn_3Sn*	65.9	12.0	22.1
							ε-$MnZn_3$**	45.2	45.6	9.2
							β-Mn[†]	76.8	21.4	1.8
2[‡]	40	50	10	38.0	49.4	12.6	new phase λ**	35.4	56.1	8.5
							Mn_2Sn**	54.8	12.8	32.4
							Mn_3Sn (4000 times)[†]	61.9	17.2	20.9
3	50	10	40	55.3	11.7	33.0	Mn_3Sn	70.5	4.8	24.7
							Mn_2Sn	55.7	10.9	33.4
4[§]	36	20	44	29.7	17.6	52.7	Mn_2Sn	53.7	8.6	37.7
							liquid (Mn_2Sn + (Sn) + $MnZn_{13}$)	17.4	22.5	60.1
5[§]	40	28	32	33.5	24.4	42.1	Mn_2Sn*	53.0	11.8	35.2
							liquid	17.6	34.1	48.3
6[§]	30	30	40	35.9	27.1	37.0	new phase λ	26.9	65.8	7.3
							Mn_2Sn	51.8	12.9	35.3
							liquid ($MnSn_2$ + (Sn) + $MnZn_{13}$)	20.6	34.0	45.4
7	55	40	5	58.1	35.4	6.5	Mn_3Sn*	69.8	8.9	21.3
							ε-$MnZn_3$*	57.7	37.7	4.6
							β-Mn*	75.4	18.5	6.1
8[#]	36	44	20	35.9	42.6	21.5	Mn_2Sn**	50.0	13.3	36.7
							new phase λ	27.0	66.4	6.6
							liquid ($MnSn_2$ + (Sn))	1.0	9.8	89.2
9	28	64	8	27.9	63.9	8.2	new phase λ*	28.0	65.0	7.0
							liquid ((Sn) + $MnSn_2$)	15.6	57.6	26.8
							Mn_2Sn*	50.8	13.0	36.2
10	80	0	20	76.0	0	24.0	Mn_3Sn*	75.7	0	24.3
							β-Mn	91.5	0	8.5
11	70	0	30	62.2	0	37.8	Mn_3Sn	75.0	0	25.0
							Mn_2Sn**	61.5	0	38.5
12	64	0	36	74.9	0	25.1	Mn_3Sn	78.1	0	21.9
							Mn_2Sn	66.7	0	33.3
13[¶]	60	0	40	64.6	0	35.4	Mn_3Sn_2	63.8	0	36.2
							Mn_2Sn			
							$MnSn_2$			
							(Sn)			
14	20	70	10	24.0	68.8	7.2	new phase λ*	25.8	70.0	4.2
							liquid* ((Sn) + $MnZn_{13}$ + $MnSn_2$)	1.5	8.9	89.6
15	57	12	31	63.5	8.6	27.9	Mn_3Sn	68.0	7.5	24.5
							Mn_2Sn	56.8	10.2	33.0
16[§]	42	14	44	44.1	8.9	47.0	Mn_2Sn	53.9	8.3	37.8
							liquid	15.8	11.9	72.3
17[§]	32	14	54	29.5	8.0	62.5	Mn_2Sn*	54.7	6.4	38.9
							liquid	12.2	8.2	79.6
18	47	30	23	47.8	25.2	27.0	new phase λ**	31.6	59.4	9.0
							Mn_2Sn**	54.8	12.5	32.7
							liquid ($MnSn_2$ + (Sn))	not determined		
19[§]	46	10	44	48.1	9.7	42.2	liquid	14.3	11.5	74.2
							Mn_2Sn	56.7	10.9	32.4
20	34	6	60	39.8	2.9	57.3	Mn_3Sn_2*	55.5	4.5	40.0
							$MnSn_2$*	34.1	1.8	64.1

*Composition is an average of at least three measurements.

**Composition is an average of two measurements.

[†]Composition was measured only once. The average composition of the alloys was measured only once by using the area scan mode. The remaining data with no superscript indication were from one measurement.

[‡]Mn_3Sn was observed by means of SEM/EDS when the magnification increased to 4000.

[§]The liquid phase was identified with SEM/EDS and XRD. X-ray diffraction suggests the phases produced from liquid during solidification.

[#]The composition of (Sn) resulting from the solidification of the liquid was measured.

[¶]The alloy was off-equilibrium. Mn_3Sn_2, Mn_2Sn, $MnSn_2$, and (Sn) could not be distinguished with SEM/EDS, and thus, an average composition of the mixture was given here.

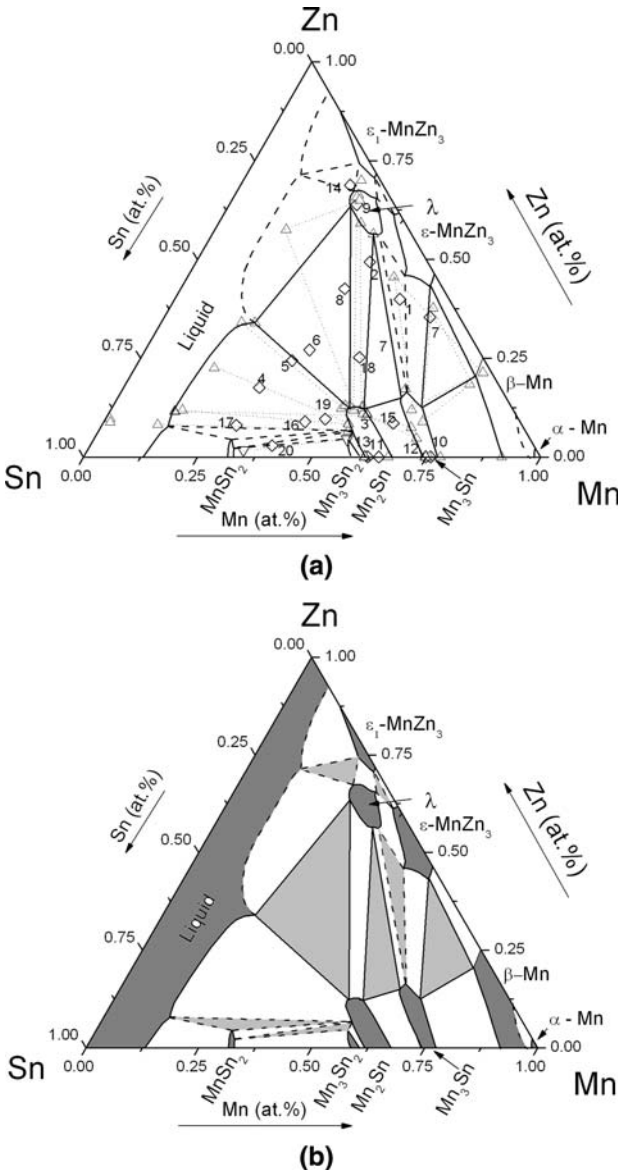

Fig. 2—Isothermal sections of the Mn-Sn-Zn ternary system at 500 °C: (*a*) with experimental data (◇: measured average compositions of alloy buttons, and △: measured compositions of related phases, which are connected with dot lines.) and (*b*) without the experimental data.

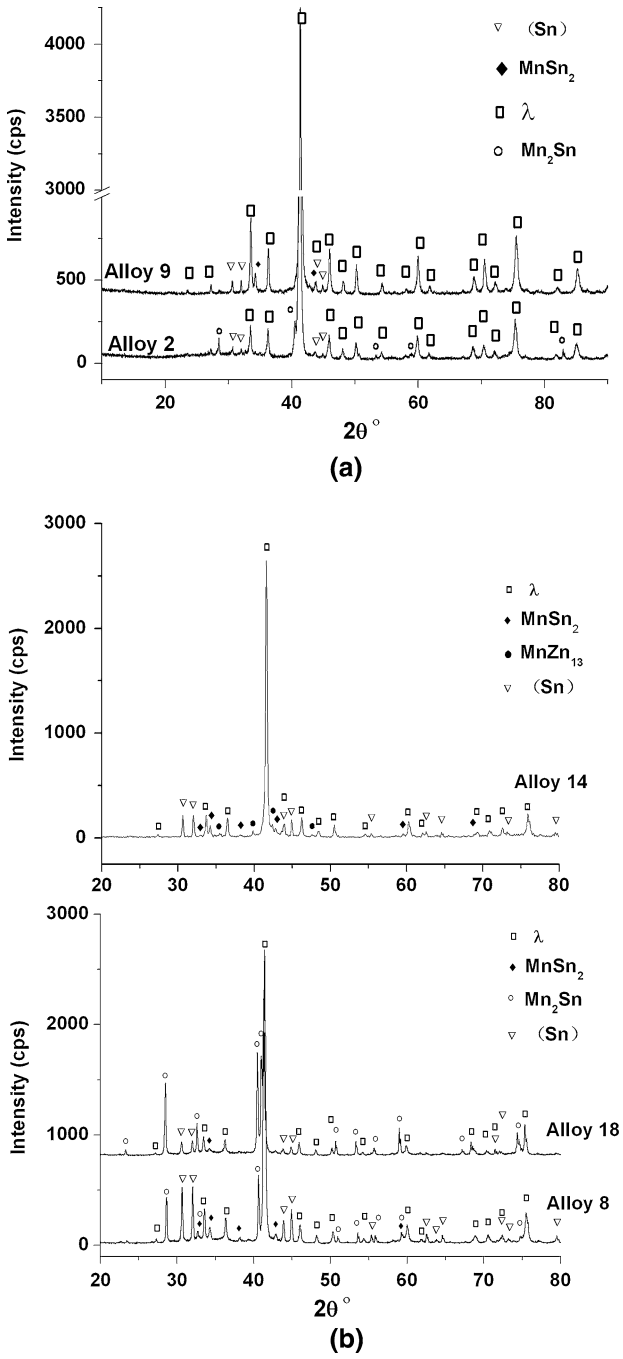

Fig. 3—Unknown diffraction peaks observed in alloys 2, 8, 9, 14, and 18. (*a*) XRD results of alloys 2 and 9 annealed at 500 °C for 20 days. (*b*) XRD results of alloys 8, 14, and 18 annealed at 500 °C for 20 days. The peaks marked in the blank square correspond to the new ternary phase (λ). The XRD patterns of alloys 2, 8, 9, and 18 were collected after the alloy powders were kept at room temperature for about 9 months by scanning in 0.02 deg and 5 s per step and filtering with graphite monochrome, while that of alloy 14 was collected in scan rate 2 deg/min.

combination of XRD and EDS. Based on Table I, the 500 °C isothermal section of the Mn-Sn-Zn system is constructed in Figure 2. A new ternary phase, denoted as λ, was identified in the present work. There exist 8 three-phase regions at 500 °C, *i.e.*, (1) β-Mn + ε-$MnZn_3$ + Mn_3Sn, (2) ε-$MnZn_3$ + λ + Mn_3Sn, (3) λ + Mn_3Sn + Mn_2Sn, (4) L + λ + Mn_2Sn, (5) ε_1-$MnZn_3$ + ε-$MnZn_3$ + λ, (6) ε_1-$MnZn_3$ + λ + L, (7) Mn_2Sn + L + $MnSn_2$, and (8) Mn_3Sn_2 + $MnSn_2$ + Mn_2Sn. Three of them, *viz.* β-Mn + ε-$MnZn_3$ + Mn_3Sn, λ + Mn_3Sn + Mn_2Sn, and L + λ + Mn_2Sn, were well determined. The remaining 5 three-phase equilibria, which were deduced, are shown with dashed lines in Figure 2.

Although the reaction of the alloys with quartz tubes was unavoidable, the EDS and XRD examination indicated that the Si contamination in the alloys was negligible.

Figures 3(a) and (b) show the XRD patterns of alloys 2, 8, 9, 14, and 18, where unknown XRD peaks were observed and marked in open squares. Besides those

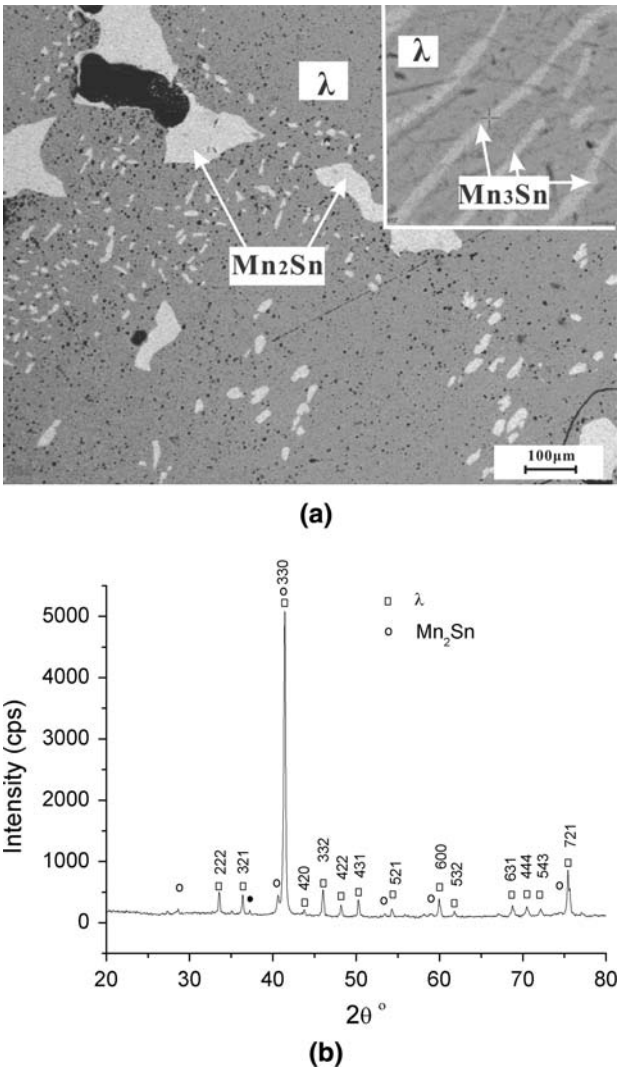

Fig. 4—(*a*) BSE image of alloy 2 annealed at 500 °C for 20 days. The gray phase is the λ phase, and the light gray phase is Mn_2Sn. The right upper corner is the image of the matrix with magnification increasing to 4000, where the matrix is the λ phase and the light gray strip is Mn_3Sn. (b) XRD patterns of alloy 2 annealed at 500 °C for 20 days. The results show no occurrence of (Sn) after direct quench. The peak marked in full circle results from diffraction of the Cu K_β radiation in the 330 plane of the λ phase, as thin Ni foil could not completely filter the Cu K_β.

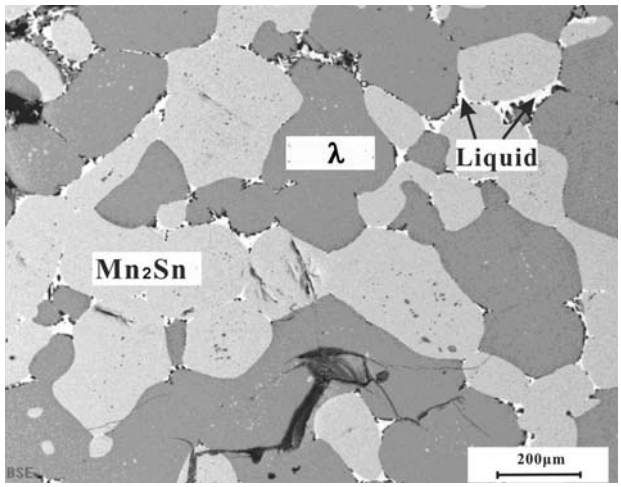

Fig. 5—BSE image of alloy 8 annealed at 500 °C for 20 days. The gray phase is Mn_2Sn, and the dark gray phase is λ. The white phase scattered between λ and Mn_2Sn is liquid.

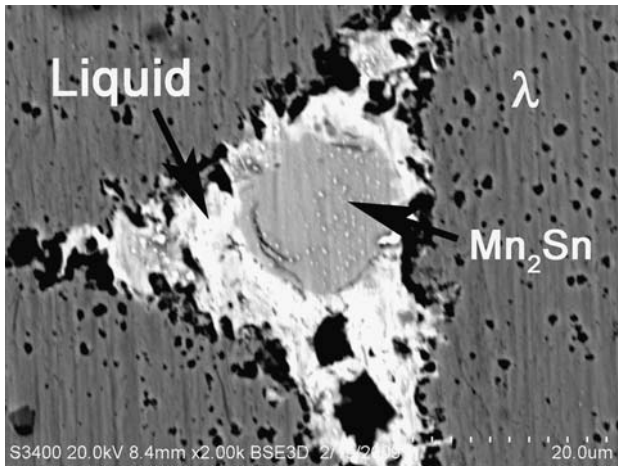

Fig. 6—BSE image of alloy 9 annealed at 500 °C for 20 days. The gray phase is Mn_2Sn, and the dark gray phase is λ. The light gray phase surrounding Mn_2Sn is liquid.

unknown peaks, the XRD also revealed the existence of Mn_2Sn and (Sn) in alloy 2, of $MnSn_2$ and Sn in alloy 9, of Mn_2Sn, $MnSn_2$, and Sn in alloys 8 and 18, and of $MnSn_2$, (Sn), and $MnZn_{13}$ in alloy 14.

Figure 4(a) is the backscattered electron (BSE) micrograph of alloy 2 under a magnification of 100 times. The composition of the light gray phase was measured to be 54.8 at. pct Mn, 32.4 at. pct Sn, and 12.8 at. pct Zn, while that of the dark phase was determined to be 35.4 at. pct Mn, 8.5 at. pct Sn, and 56.1 at. pct Zn. Combining the microstructure and XRD results of alloy 2, it could be concluded that the light gray phase in Figure 4(a) is Mn_2Sn. Those unknown peaks in Figure 3(a) should belong to the unidentified dark phase in Figure 4(a), the composition of which is close to the boundary Mn-Zn binary system. Since the unknown peaks in Figure 3(a) did not match any equilibrated phases in the Mn-Zn binary system at 500 °C, a new ternary phase, referred to as λ, was assumed to exist in this ternary system at 500 °C. Further investigation on alloys 8, 9, and 18 substantiates this conclusion, as discussed subsequently.

Figures 5 through 7 show the microstructures of alloys 8, 9, and 18. The compositions of the new ternary phase (λ) were measured to be 27.0 at. pct Mn, 6.6 at. pct Sn, and 66.4 at. pct Zn for alloy 8, to be 28.0 at. pct Mn, 7.0 at. pct Sn, and 65.0 at. pct Zn for alloy 9, and to be 31.6 at. pct Mn, 9.0 at. pct Sn, and 59.4 at. pct Zn for alloy 18, respectively. The λ phase was found to occupy a large volume fraction in alloy 9, which is in accord with its great XRD intensity. It is worth noting that the XRD pattern of alloy 18 indicated the existence of (Sn) and $MnSn_2$ in this alloy, but they were not

observed *via* the SEM examination. Thus, no compositions for them were listed in Table I.

As listed in Table I, the composition range of the new ternary phase (λ) was measured to span from about 25 to 35 at. pct Mn, 4 to 8 at. pct Sn, and 55 to 70 at. pct Zn. Thus, a formula Mn_4Zn_8Sn is deduced for this phase.

The crystal structure of the new ternary phase (λ) was determined with alloy 9 to be of a bcc structure with a lattice parameter $a = 0.92508$ (5) nm, as shown in Table II, indexed by employing program Treor.[29] Using the program Dicvol[30] packed in Fullprof[31] yielded the same results. It should be mentioned that the binary compound Mn_5Zn_{21}, which congruently melts at about 420 °C[18] and also has a bcc structure with a lattice parameter $a = 0.916$ nm, is near the λ phase on the 500 °C isothermal section. So, this ternary phase (λ) could be supposed to be the Mn_5Zn_{21} phase stabilized by the addition of the third element Sn at elevated temperatures.

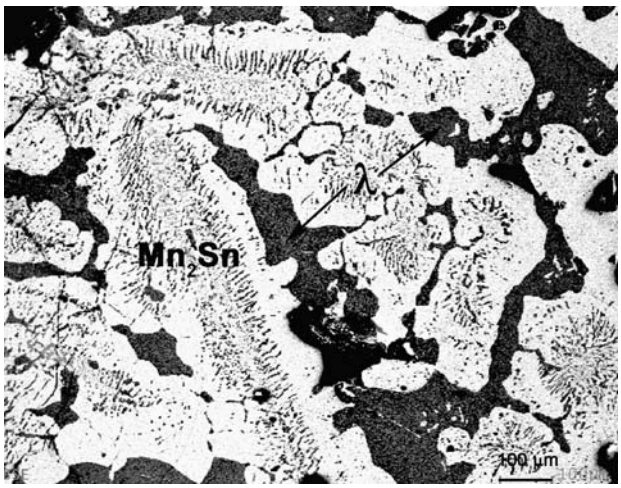

Fig. 7—Microstructure of alloy 18 annealed at 500 °C for 20 days. The white phase is Mn_2Sn, and the dark phase is λ. The EDS revealed strip hold scattering in the Mn_2Sn matrix is the λ.

Mn_3Sn was observed in alloy 2 when the magnification increased to 4000 times, as shown in the right upper corner of Figure 4(a). The light gray strip was identified as Mn_3Sn, whose composition was measured to be 61.9 at. pct Mn, 20.9 at. pct Sn, and 17.2 at. pct Zn. This phase occupied a trace amount of volume fraction, and its XRD intensity was too weak to be detected. It is worth noting that the detected (Sn) for alloy 2 in Figure 3(a) could be regarded as the segregated phase after the alloy was kept at room temperature for about 9 months since it was not observed when the alloy was subjected to direct quench. The XRD pattern of this alloy after direct quench is displayed in Figure 4(b).

Figures 8(a) and (b) present the XRD pattern and microstructure of alloy 6. As shown in Figure 8(b), the white phase was identified as Mn_2Sn and the dark phase surrounding Mn_2Sn identified as λ. The matrix is the mixture of $MnSn_2$, Sn, and $MnZn_{13}$, which was produced from the slow quenching process and should be the liquid at 500 °C. The compositions of the λ and Mn_2Sn in alloys 6, 8, and 9 were measured to be close to each other correspondingly, as listed in Table I. According to the present work, alloys 6, 8, and 9 are located in the three-phase equilibrium region of $\lambda + Mn_2Sn +$ liquid, though the compositions of the liquid in alloys 6, 8, and 9 were measured to be significantly different. It should be mentioned that the liquid composition for alloy 6 was measured with the area scan mode, while those for alloys 8 and 9 were measured with the point mode. Since the liquid transformed into the mixture of $MnSn_2$, (Sn), and $MnZn_{13}$ after solidification, it is more reasonable to take the result of the area measurement as the actual composition. So, only the measured

Table II. Indexing Results of the New Ternary Phase in Alloy 9 by Using Program Treor[30]

H	*K*	*L*	$\sin^2\theta$-Obs.	$\sin^2\theta$-Calc.	Delta	2θ-Obs.	2θ-Calc.	*d*-Obs.(nm)	I/I_0
2	1	1	0.041477	0.041601	–0.000125	23.502	23.538	0.3782	0.4
2	2	0	0.055447	0.055469	–0.000021	27.239	27.244	0.3271	1.1
2	2	2	0.083233	0.083203	0.00003	33.537	33.53	0.2670	10.1
3	2	1	0.097036	0.09707	–0.000034	36.300	36.307	0.2473	5.9
3	3	0	0.124714	0.124804	–0.000091	41.360	41.376	0.2181	100
4	2	0	0.138607	0.138672	–0.000065	43.715	43.726	0.2069	1.4
3	3	2	0.152426	0.152539	–0.000113	45.961	45.979	0.1973	6.8
4	2	2	0.166467	0.166406	0.000061	48.159	48.15	0.1888	2.4
5	1	0	0.180213	0.180273	–0.00006	50.240	50.249	0.1815	4.3
5	2	1	0.207953	0.208007	–0.000054	54.261	54.269	0.1689	2.1
6	0	0	0.249698	0.249609	0.000089	59.960	59.948	0.1542	7.4
6	1	1	0.263563	0.263476	0.000087	61.779	61.768	0.1500	1.6
6	3	1	0.318862	0.318944	–0.000082	68.760	68.77	0.1364	3.3
4	4	4	0.332932	0.332812	0.00012	70.480	70.465	0.1335	6.2
7	1	0	0.34682	0.346679	0.000141	72.160	72.143	0.1308	2.2
7	2	1	0.374633	0.374413	0.000219	75.479	75.453	0.1259	14
6	5	1	0.429731	0.429882	–0.000151	81.921	81.938	0.1175	1.7
8	1	1	0.457465	0.457616	–0.000151	85.120	85.137	0.1139	6.5

Indexing merit: M (18) = 34, and F (18) = 18.

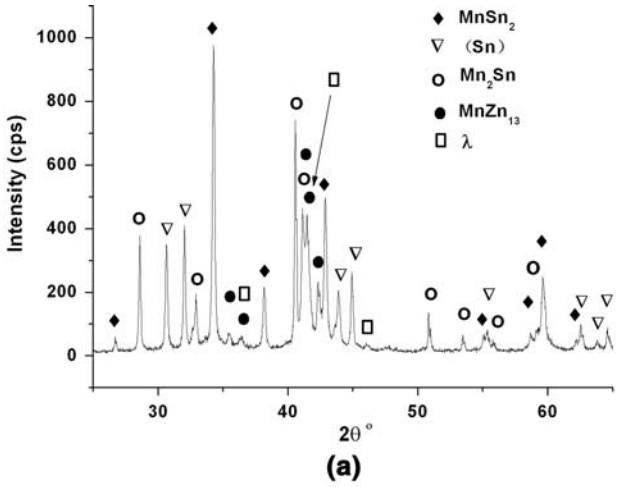

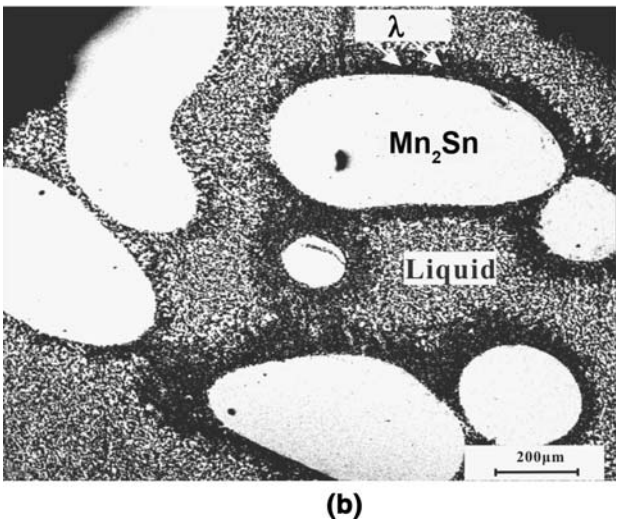

Fig. 8—(*a*) XRD results of alloy 6 annealed at 500 °C for 20 days. λ, Mn_2Sn, (Sn), $MnZn_{13}$, and $MnSn_2$ were identified. The XRD was conducted after the alloy powder had been kept at room temperature for 9 months by scanning in 0.02 deg and 5 s per step, and filtering with graphite monochrome. (*b*) Microstructure of alloy 6 annealed at 500 °C for 20 days. The white phase is Mn_2Sn, and the black phase surrounding Mn_2Sn is λ. The matrix is liquid.

composition of the liquid in alloy 6 was considered in the construction of the tie-triangle of λ + Mn_2Sn + liquid.

Liquid and Mn_2Sn were observed in alloys 4, 5, 16, and 17. Due to the solidification segregation of the liquid phase during its quenching process, the identification of the liquid phase mainly depends on both the observed microstructure and compositional analysis. The microstructures of alloys 5 and 16 are shown in Figures 9 and 10, respectively. For alloy 5, Mn_2Sn and (Sn) together with $MnSn_2$ and $MnZn_{13}$ were detected at room temperature *via* XRD, as shown in Figure 11. The light gray phase was scattered like an island in the matrix of alloy 5, as shown in Figure 9. Its composition was measured to be 53.0 at. pct Mn, 35.2 at. pct Sn, and 11.8 at. pct Zn. This phase was identified as Mn_2Sn. And the matrix, which showed uniform microstructure under low magnification, was composed of $MnSn_2$ and (Sn) together with $MnZn_{13}$. The composition of the matrix

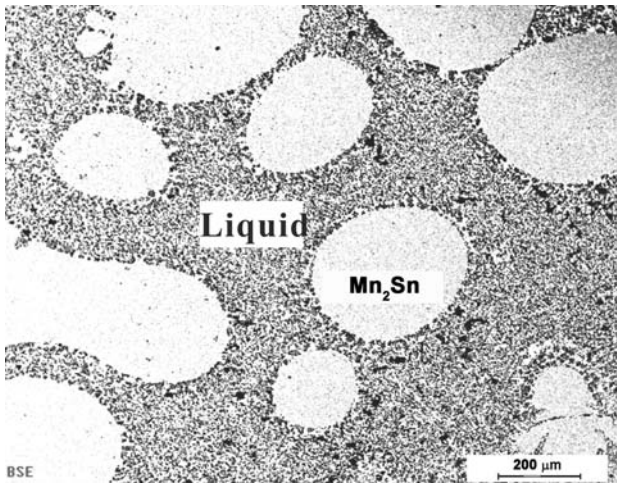

Fig. 9—Microstructure of alloy 5 annealed at 500 °C for 20 days. The matrix is liquid, and the light gray phase is Mn_2Sn.

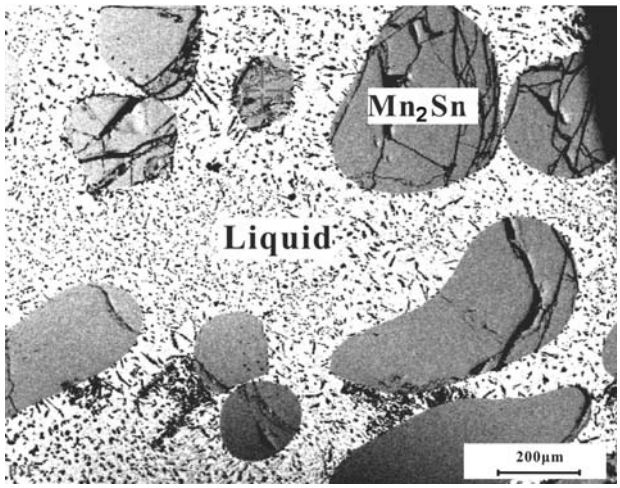

Fig. 10—Microstructure of alloy 16 annealed at 500 °C for 20 days. The dark phase is Mn_2Sn, and the matrix is liquid.

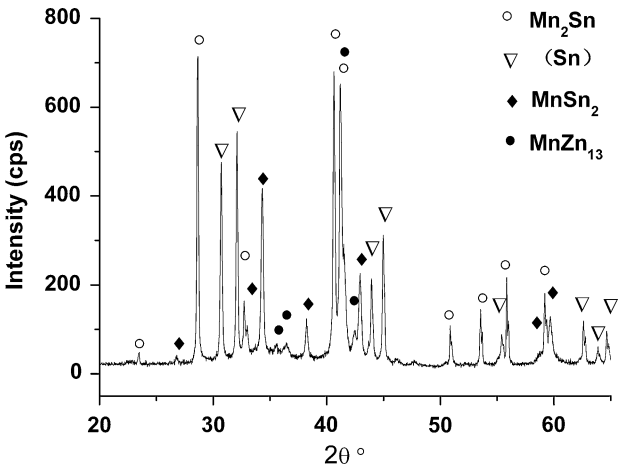

Fig. 11—XRD result of alloy 5 annealed at 500 °C for 20 days and held at room temperature for about 9 months. Step scan: 0.02 deg and 5 s per step, graphite monochrome.

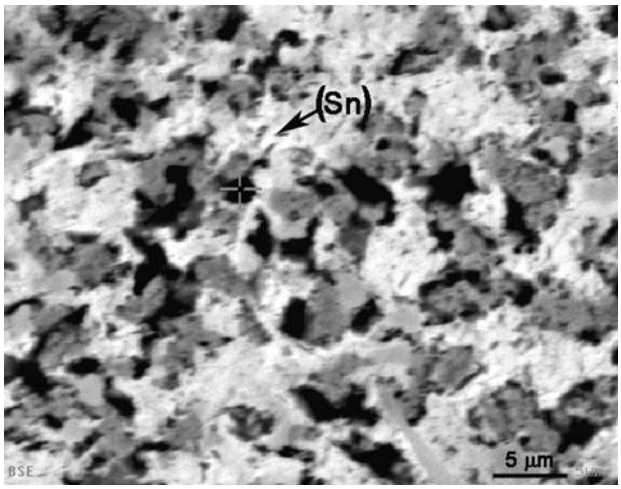

Fig. 12—Microstructure of the matrix in alloy 5 annealed at 500 °C for 20 days, showing the random distribution of the phases resulting from the solidification of the liquid.

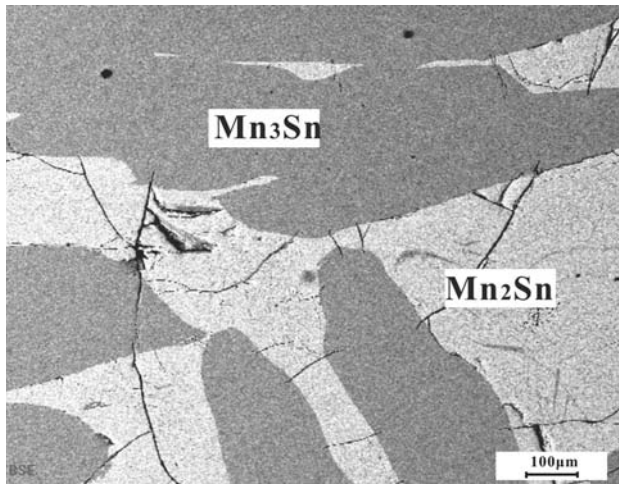

Fig. 13—Microstructure of alloy 12 annealed at 500 °C for 20 days. The dark phase is Mn_3Sn, and the gray phase is Mn_2Sn.

Table III. Compositions of (Sn) and $MnSn_2$ Measured in Alloys 4, 8, 9, 19, and 20

		Phase Composition (At. Pct)		
Number	Phases	Sn	Mn	Zn
4	(Sn)	91.6	2.2	6.2
8	(Sn)	89.2	1.0	9.8
9	(Sn)	85.5	3.2	11.3
	$MnSn_2$	62.3	5.8	31.9
19	(Sn)	82.6	1.0	16.4
	$MnSn_2$	63.9	32.0	4.1
20*	(Sn)	85.3	1.5	13.2

*(Sn) in alloy 20 precipitates from $MnSn_2$.

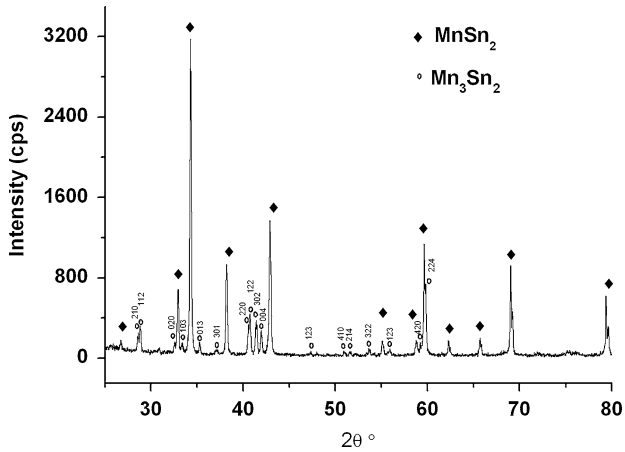

Fig. 14—XRD patterns of alloy 20 annealed at 500 °C for 20 days, showing the coexistence of Mn_3Sn_2 and $MnSn_2$.

was roughly measured to be 17.6 at. pct Mn, 48.3 at. pct Zn, and 34.1 at. pct Sn. Further SEM examination revealed that the matrix consisted of gray, dark, white, and light gray phases, as shown in Figure 12. The phases distributed randomly with irregular shape in the matrix might result from the rapid solidification of liquid. Only the composition of the white phase in the matrix was measured, and a value of 91.6 at. pct Sn, 6.2 at. pct Zn, and 2.2 at. pct Mn was obtained. This phase was identified as (Sn). As shown in Table III, the similar compositions of (Sn) were detected in alloys 4, 8, and 9. It is worth noting that the compositions of (Sn) in those alloys were close to the Sn-Zn eutectic composition. Thus, it could be reasonably concluded that (Sn) was a solidification product of the liquid. Since the (Sn) phase is mixed randomly with $MnSn_2$ and $MnZn_{13}$, it could be deduced that $MnSn_2$ and $MnZn_{13}$ were also the products of the quenched liquid. Hence, it was also concluded that the matrix in alloy 5 should be the liquid at 500 °C.

Figure 13 is the micrograph of alloy 12. Mn_3Sn is in phase equilibrium with Mn_2Sn, which is consistent with the phase diagram presented by Stange *et al.*[26] The same phase assemblage as that in alloy 12 was observed in alloys 3, 11, and 15. A significant weight loss was observed for alloys 11 and 12 during the melting process. The weight loss for the alloys containing Mn and Zn is inevitable due to the high evaporability of Mn and Zn at high temperatures. To ensure that the conclusion is reliable, the measured compositions of the alloys rather than the nominal compositions were considered in the phase diagram construction.

The existence of Mn_3Sn_2 was separately reported by two research groups.[26,27] However, later investigation on the Ti-Mn-Sn and V-Mn-Sn systems indicated no existence of Mn_3Sn_2 at 497 °C.[32,33] In the present work, the equilibrium between Mn_3Sn_2 and $MnSn_2$ was observed in alloy 20, which was subjected to direct quench, as shown in Figure 14. After being kept at room temperature for about 9 months, the alloy was examined with SEM/EDS again. Mn_3Sn_2 and $MnSn_2$ were observed together with additional (Sn), which precipitated

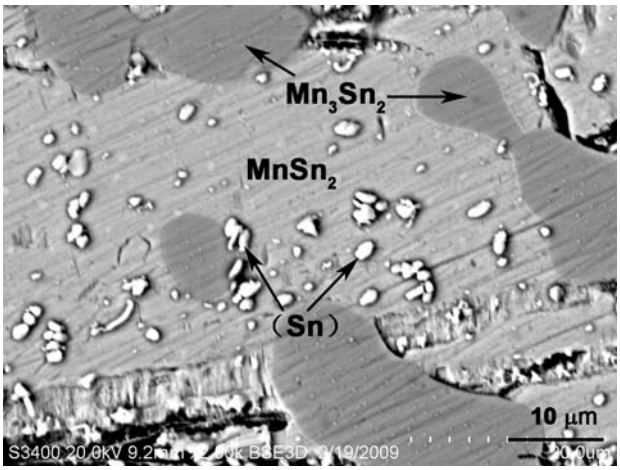

Fig. 15—Microstructure of alloy 20 annealed at 500 °C for 20 days and kept at room temperature for about 9 months. The gray phase is Mn_3Sn_2, the light gray phase is $MnSn_2$, and the white point scattered in $MnSn_2$ is (Sn).

in the $MnSn_2$ matrix, as shown in Figure 15. Similar results were reported in Reference 27. The interpretation presented by Elding-Pontén *et al.*[27] is that $MnSn_2$ is not a line compound and the supersaturated Sn in $MnSn_2$ would dissolve out at low temperature. The present experimental results supported this viewpoint. It was found that the tie-line between Mn_3Sn_2 and Mn_2Sn is difficult to determine, as Mn_2Sn and Mn_3Sn_2 have close compositions and show little color contrast. Consequently, they were not distinguished from each other by SEM/EDS in alloy 13, though Mn_2Sn and Mn_3Sn_2 together with a trace amount of $MnSn_2$ and (Sn) had been identified by XRD.

According to the experimental results summarized in Table I, the maximum solubilities of Zn in Mn_3Sn, Mn_2Sn, and Mn_3Sn_2 at 500 °C are about 17, 12, and 4 at. pct, respectively.

IV. CONCLUSIONS

The phase equilibria at 500 °C in the Mn-Sn-Zn ternary system were investigated by means of XRD and SEM/EDS, using equilibrated alloys. In the 500 °C isothermal section, there exist 8 three-phase regions: (1) β-Mn + ε-$MnZn_3$ + Mn_3Sn, (2) ε-$MnZn_3$ + λ + Mn_3Sn, (3) λ + Mn_3Sn + Mn_2Sn, (4) L + λ + Mn_2Sn, (5) ε_1-$MnZn_3$ + ε-$MnZn_3$ + λ, (6) ε_1-$MnZn_3$ + λ + L, (7) Mn_2Sn + L + $MnSn_2$, and (8) Mn_3Sn_2 + $MnSn_2$ + Mn_2Sn. Three of them, *i.e.*, β-Mn + ε-$MnZn_3$ + Mn_3Sn, λ + Mn_3Sn + Mn_2Sn, and L + λ + Mn_2Sn, are well established.

One ternary phase, with a formula of Mn_4Zn_8Sn, was identified with a bcc structure and a lattice parameter of $a = 0.92508$ (5) nm. Its composition range is about 25 to 35 at. pct Mn, 4 to 8 at. pct Sn, and 56 to 70 at. pct Zn.

The binary $MnZn_3$, Mn_3Sn, Mn_2Sn, and Mn_3Sn_2 phases were observed to be stable at 500 °C. The maximum solubilities of Zn in Mn_3Sn, Mn_2Sn, and Mn_3Sn_2 are about 17, 12, and 4 at. pct, respectively.

The coexistence of liquid with Mn_2Sn was observed in several alloys. The liquid transformed into $MnSn_2$, (Sn), and $MnZn_{13}$ during solidification.

ACKNOWLEDGMENTS

This work is supported by the National Natural Science Foundation of China (Grant Nos. 50721003 and 50831007), the Guangxi Science Foundation (Contract Nos. 0448022, 0540009, and 0640040), Guangxi Large Scale Apparatus Corporation Office, and the National Outstanding Youth Science Foundation of China (Grant No. 50425103). Thanks are also due to Mrs. J.R Huang for SEM/EDS examination.

REFERENCES

1. N.Y. Tang: *J. Phase Equilib.*, 2008, vol. 29, pp. 337–44.
2. G. Reumont, P. Perrot, and J. Foct: *J. Mater. Sci.*, 1998, vol. 33, pp. 4759–68.
3. N. Pistofidis, G. Vourlias, S. Konidaris, E. Pavlidou, A. Stergiou, and G. Stergioudis: *Mater. Lett.*, 2006, vol. 60, pp. 786–89.
4. N. Pistofidis, G. Vourlias, E. Pavlidou, K. Chrissafis, G. Stergioudis, E.K. Polychroniadis, and D. Tsipa: *J. Therm. Anal. Calorim.*, 2006, vol. 86, pp. 417–22.
5. G. Reumont, T. Gloriant, and P. Perrot: *J. Mater. Sci. Lett.*, 1996, vol. 15, pp. 445–49.
6. R.W. Sandelin: *Wire Wire Products*, 1940, vols. 15–11, pp. 655–76.
7. N.Y. Tang: *J. Phase Equilib.*, 2006, vol. 27, pp. 462–68.
8. N.Y. Tang, X.P. Su, and J.M. Toguri: *CALPHAD*, 2001, vol. 25, pp. 267–77.
9. N.Y. Tang, X.P. Su, and X.B. Yu: *J. Phase Equilib.*, 2003, vol. 24, pp. 528–32.
10. X.H. Tang, F.C. Yin, X.M. Wang, J.H. Wang, X.P. Su, and N.Y. Tang: *J. Phase Equilib.*, 2007, vol. 28, pp. 355–61.
11. N.Y. Tang and X.P. Su: *Metall. Mater. Trans. A*, 2002, vol. 33A, pp. 1559–61.
12. G. Reumont, G. Dupont, and P. Perrot: *Z. Metallkd.*, 1995, vol. 86, pp. 608–13.
13. G. Reumont, M. Mathon, R. Fourmentin, and P. Perrot: *Z. Metallkd.*, 2003, vol. 94, pp. 411–18.
14. Y.X. Liu, F.C. Yin, H. Tu, Z. Li, J. Wang, and X.P. Su: *J. Phase Equilib.*, 2008, vol. 29, pp. 493–99.
15. Z.H. Wang, J.H. Wang, Y.H. Liu, N.Y. Tang, and X.P Su: *J. Phase Equilib.*, 2006, vol. 27, pp. 469–76.
16. G. Reumont, T. Gloriant, and P. Perrot: *J. Mater. Sci. Lett.*, 1997, vol. 16, pp. 62–65.
17. S.W. Pan, F.C. Yin, M.X. Zhao, Y. Liu, and X.P. Su: *J. Alloys Compd.*, 2009, vol. 470, pp. 600–05.
18. H. Okamoto and L.E. Tanner: *Bull. Alloy Phase Diagrams*, 1990, vol. 11, pp. 377–84.
19. E. Wachtel and K. Tsiuplakis: *Z. Metallkd.*, 1967, vol. 58, pp. 41–45.
20. J. Schramm: *Z. Metallkd.*, 1940, vol. 32, pp. 399–407.
21. E.V. Potter and R.W. Huber: *Trans. ASM*, 1949, vol. 41, pp. 1001–22.
22. W.B. Henderson and R.J.M. Willcox: *Philos. Mag.*, 1964, vol. 9, pp. 829–46.
23. O. Romer and E. Wachtel: *Z. Metallkd.*, 1971, vol. 62, pp. 820–25.
24. Y. Nakagawa and T. Hori: *Trans. Jpn. Inst. Met.*, 1972, vol. 13, p. 167.
25. H.H. Xu, X. Xiong, L.J. Zhang, Y. Du, and P.S. Wang: *Metall. Mater. Trans. A*, 2009, vol. 40A, pp. 2042–47.
26. M. Stange, H. Fjellvåg, S. Furuseth, and B.C. Hauback: *J. Alloys Compds.*, 1997, vol. 259, pp. 140–44.
27. M. Elding-Pontén, L. Stenberg, A.K. Larsson, S. Lidin, and K. Ståhl: *J. Solid State Chem.*, 1997, vol. 129, pp. 231–41.

28. Z. Moser, J. Dutkiewicz, W. Gasior, and J. Salawa: *Bull. Alloy Phase Diagrams*, 1985, vol. 6, pp. 330–34.
29. P.-E. Werner, L. Eriksson, and M. Westdahl: *J. Appl. Cryst.,* 1985, vol. 18, pp. 367–70, http://www.ccp14.ac.uk/ccp/ccp14/ccp14-by-program/treor/ccp14-expanded/treor90-dos/.
30. A. Boultif and D. Louër: *J. Appl. Crystallogr.*, 2004, vol. 37, pp. 724–31.
31. J. Rodríguez-Carvajal: FullProf, http://www-llb.cea.fr/fullweb/powder.htm, 2009.
32. A.V. Tkachuk, L.G. Akselrud, Y.V. Stadnyk, and O.I. Bodak: *J. Alloys Compds.*, 2000, vol. 312, pp. 284–87.
33. A.V. Tkachuk, Y.K. Gorelenko, Y.V. Stadnyk, and O.I. Bodak: *J. Alloys Compds.*, 2001, vols. 317–318, pp. 280–83.